5-9-2012

Preproduction Silicon Strip-pixel Sensor Testing for the Phenix VTX upgrade

Douglas E. Fields

C. Hagemann

M. Hoeferkamp

M.D. Malik

J. Turner

See next page for additional authors

Preproduction Silicon Strip-pixel Sensor Testing for the Phenix VTX upgrade

C.Hägemann, M.Hoeferkamp, D.E.Fields,
M.D.Malik, J.Turner, A.Zimmerman
New Mexico Center for Particle Physics
University of New Mexico, Albuquerque

April 14, 2006

Abstract

This document describes in detail the testing performed on some of the preproduction silicon sensors for the Phenix VTX upgrade. The results obtained at the University of New Mexico between May 2005 and March 2006 are presented. Experimental results of static measurements of leakage current and depletion voltage, as well as laser induced pulseheight are presented. Measurements were made before and after irradiation with fluences relevant to RHIC experiments.

1 Introduction

The University of New Mexico (UNM) group joined the Phenix VTX upgrade effort to help in the quality assurance (QA) testing of the production sensors. The other groups involved in the testing are at Brookhaven National Lab (BNL) and Stony Brook University (SBU). As part of the QA team, some preproduction sensors were given to the group to setup a teststand and identify any neccessary design changes for the production. One wafer with 3 sensors and 6 test photo diodes was received by the group in May 2005 and all the testing described in the following was performed on these sensors (diodes).
Initially the testing was focused on the sensors at hand, which were diced out of the wafer by Micro Dicing Technology Inc. in California. After all the neccessary measurements were performed, UNM lead the effort of studying the effect of irradiation on the sensors. Two sensors and two diodes were irradiated at the Indiana University Cyclotron Facility (IUCF). All the post irradiation measurements were performed at UNM.
The goal of all the studies performed was to understand the sensors in full detail, to identify any design changes to the sensors and to set up a detailed QA testing plan for the production sensors.

2 Prototype Sensors

All the measuremts presented were performed on a $500\mu m$ preproduction sensor with identification B2W15 sensor 1 (s1), sensor 2 (s2) and sensor 3 (s3). The sensors were fabricated by Hamamatsu Photonics/Japan. A schematic of the sensor is shown in figure (1). The number of readout strips per sensor is 128

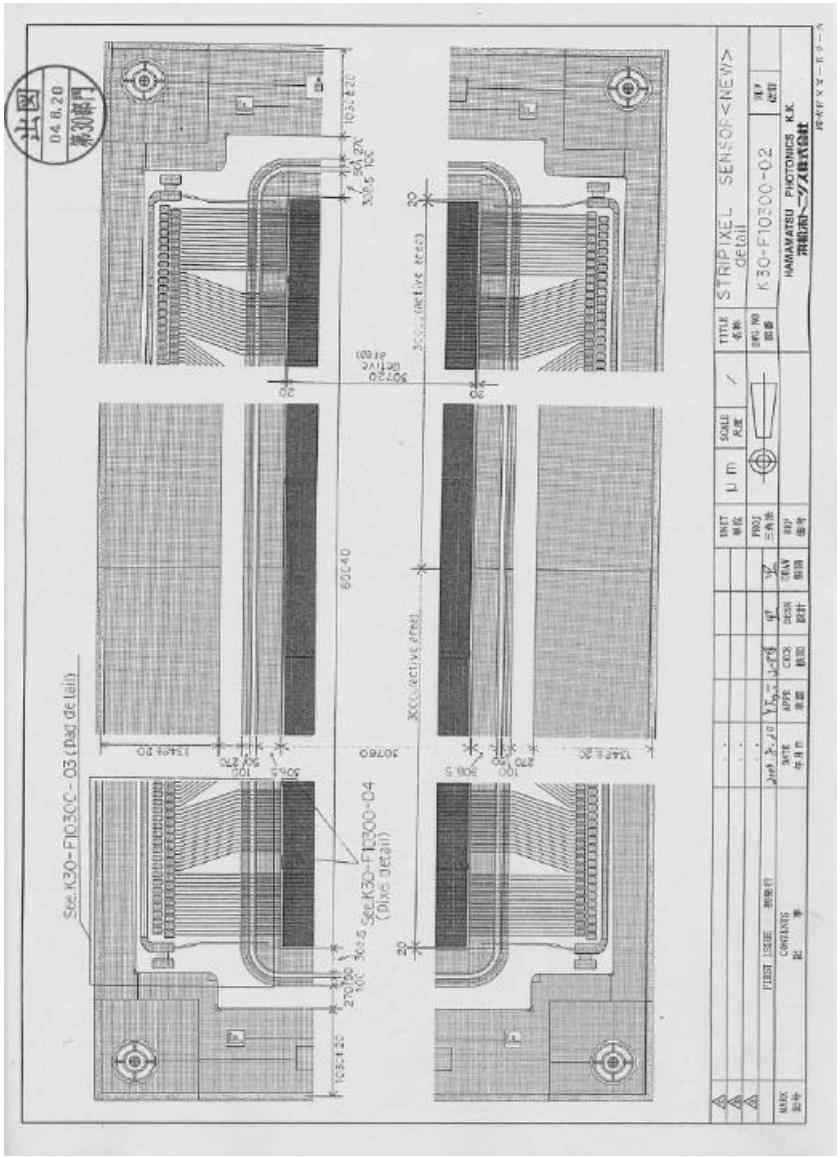

Figure 1: The VTX preproduction Si sensor

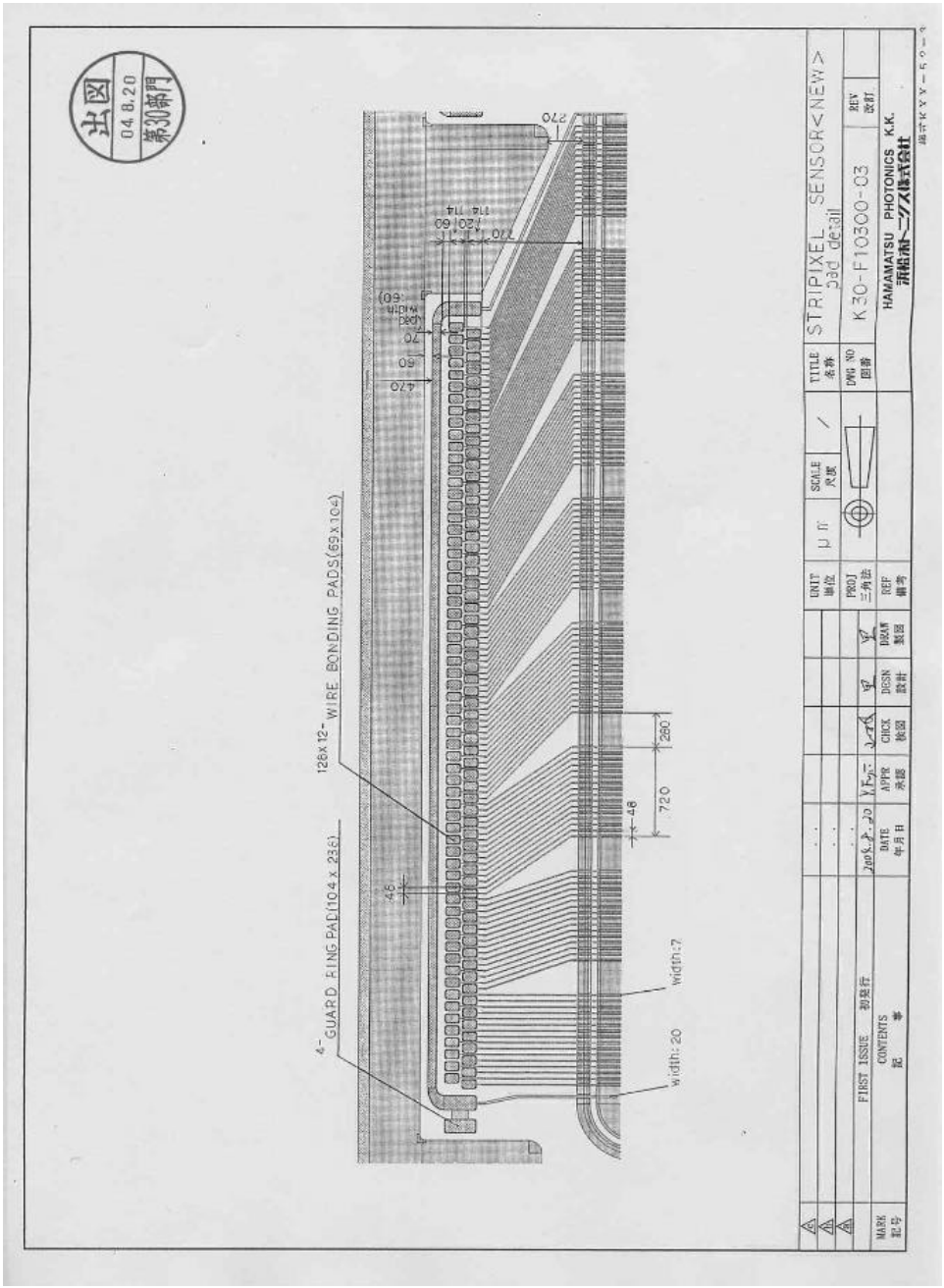

Figure 2: Detail of the design of the readout pads

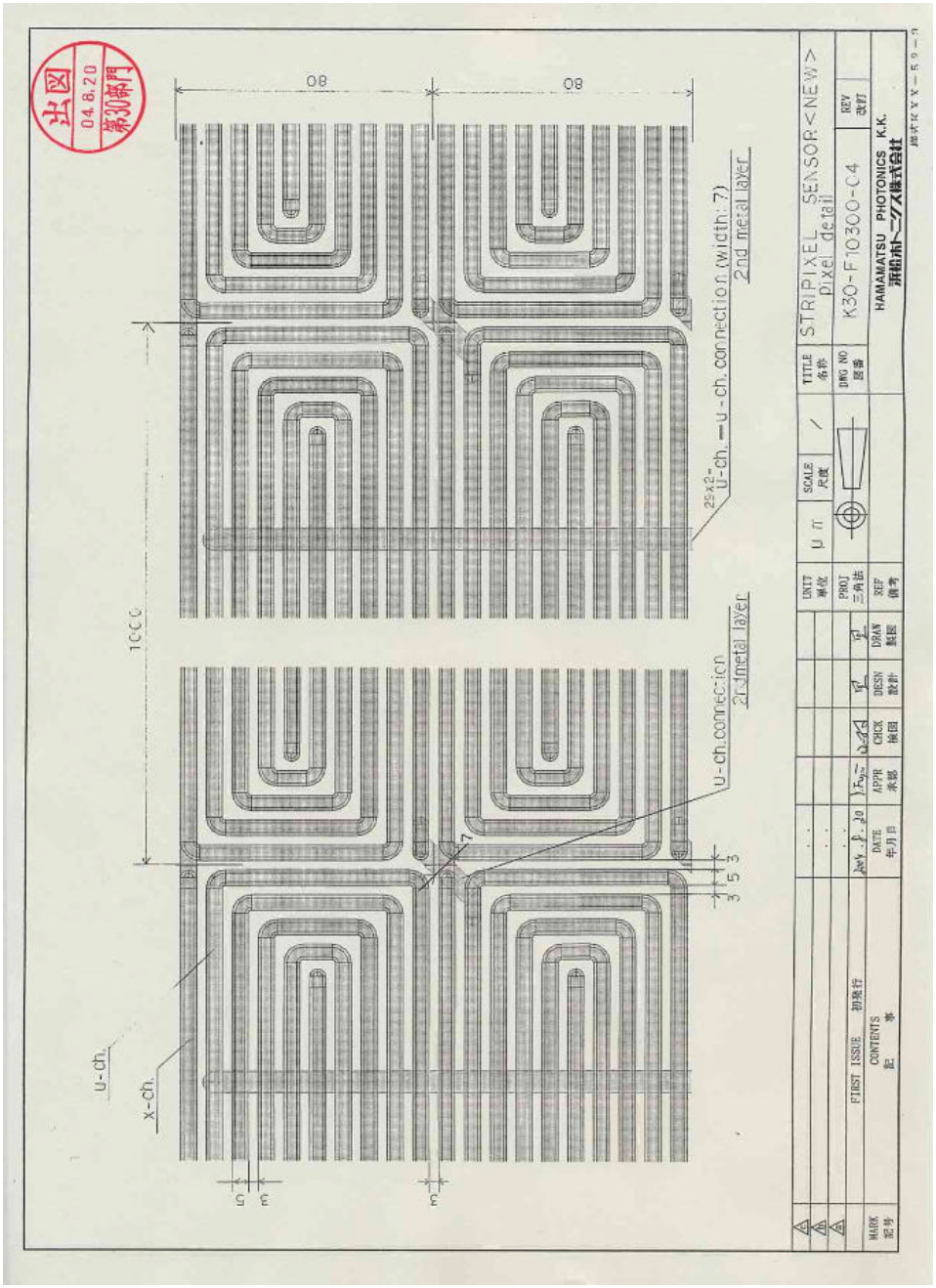

Figure 3: Detail of the design of the pixel

strip-pixels per set of read-out pads x 12 sets per sensor = 1536 strips [1].

3 The Testing Program

The complete testing program for the VTX Phenix upgrade preproduction Si strip-pixel sensors is described in the following. The testing of the sensors consisted of:

1. Visual inspection
2. Mechanical measurements
3. Electrical Measurement

3.1 Visual Inspection

The visual inspection of all received sensors/wafers ensures that the sensor is free from physical defects and scratches. The results of the visual inspection should point out defects in the region of the pads, strip region, guard ring and edges (if sensors have already been diced out of the wafer). This is to ensure further electrical testing on these regions to determine the effect, if any, of the physical defect on the sensor performance. The visual inspection is conducted on a x-y moving table with a microscope having at least 1:60 magnifying optics. A camera is hooked up to the microscope to enable recording of the defects in a file for future reference. The sensor would not have been measured if severe scratching is discovered or the dicing has inflicted major damage to the sensor. On the wafer at hand, wafer B2W15, no major damage or severe scratching was found by the visual inspection; neither before nor after the dicing procedure.

3.2 Mechanical Measurements

Mechanical Measurements of the wafer B2W15 were performed using an Eichhorn + Hausmann MX 203-6-33 contactless wafer thickness and geometry gauge. This instrument uses 17 no contact probes to measure the local thickness and the local warp of the wafer. The results are summarized in the following table and are also shown in fig.(4):

Thickness (μm):	Average	Maximum	Minimum
	499.1	501.8	496.7
Warp (μm):	Average	Maximum	Minimum
	0.001	17.7	-17.3

The results indicate that the wafer is very smooth and there should not be any problems with measuring this sensor with the probecard. As a general measure, a maximum deviation of 5% from the average thickness and the average warp should not be exceeded for a wafer to pass the mechanical measurement.

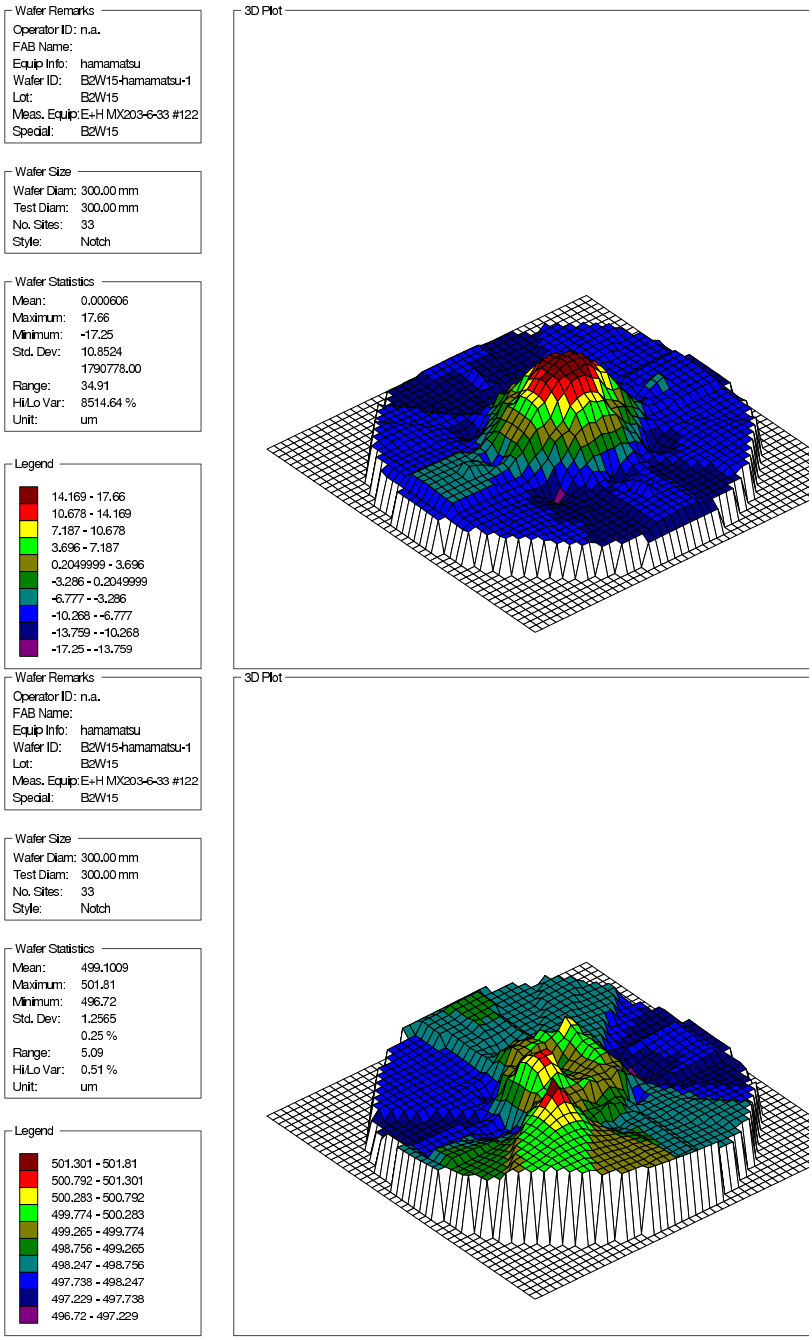

Figure 4: Local Warp and Local Thickness of wafer B2W15

3.3 Electrical Measurements

There are four different electrical measurements performed on the silicon sensors. A measurement of the leakage current I_{Leak} and the capacitance C_{Strip} is performed at a fixed bias voltage V_{Bias} on every channel out of a set of 128. These measurements determine the leakage current and capacitance values of the sensor and enable the identification of bad channels. The second set measures the leakage current and the capacitance versus bias voltage V_{Bias}. From these measurements the breakdown V_{Break} and the depletion voltage V_{Depl} are found.
The IV and CV measurements are also performed on the diodes and give an estimate of what to expect for Breakdown and Depletion Voltage when measuring the sensors. These results are not discussed in detail as the interest is focused on the behaviour of the sensors, not the diodes. Two characteristic IV and CV plots are nevertheless shown in fig.(5) and (6).

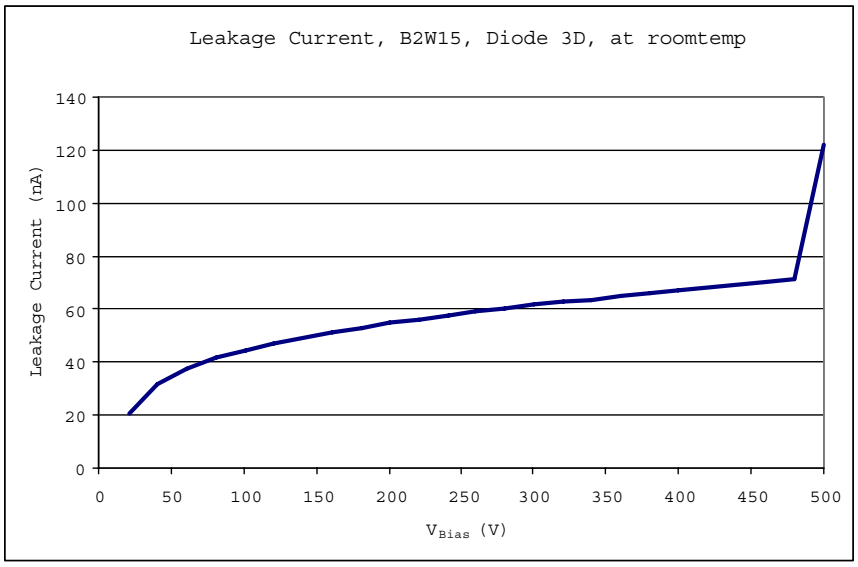

Figure 5: Characteristic IV measurement on the Testdiode

The probestation setup for the sensor measurements is shown in fig.(7).

The LCR meter is connected to the scanner when measuring capacitance, the ammeter when measuring current. The different scanner channels are connected via a ribbon cable to the probecard. The probecard has 128 needles to readout one set of pads at a time from the sensor. The scanner closes a certain channel and therefore reads out only one strip-pixel of the sensor at a time. During this measurement the other 127 channels are connected to ground. As the sensor is DC coupled, without any bias resistors on the sensor, only the area of the sensor that is probed is grounded and therefore depleted of charge carriers. The rest of

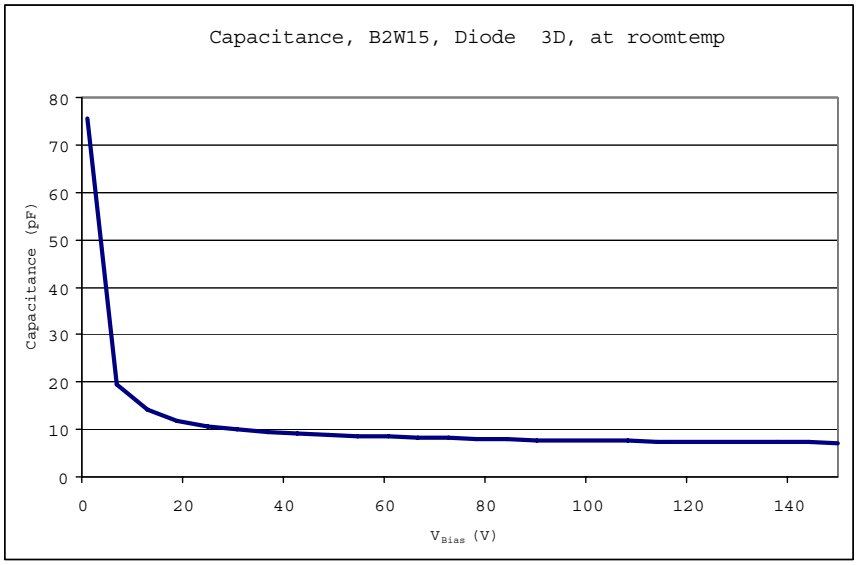

Figure 6: Characteristic CV measurement on the Testdiode

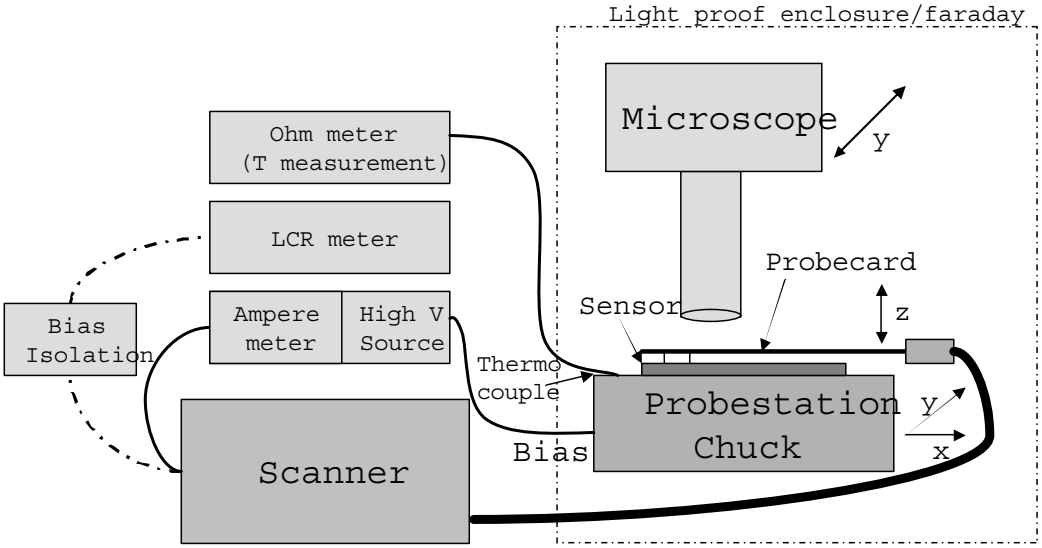

Figure 7: Setup of the Probestation

the sensor is "floating" as it is not biased. This is an issue that was addressed and is discussed in detail in section 4.1.

3.3.1 Finding the Breakdown Voltage V_{Break}

The Breakdown Voltage of the sensor needed to be determined first, to make sure that the capacitance measurements were only performed at $V_{Bias} < V_{Break}$. To find V_{Break}, the leakage current was measured as a function of V_{Bias} on one channel out of 128 at a time. 4 out of the 128 channels per set of pads were chosen to be measured. A characteristic measurement is shown in fig.(8). The

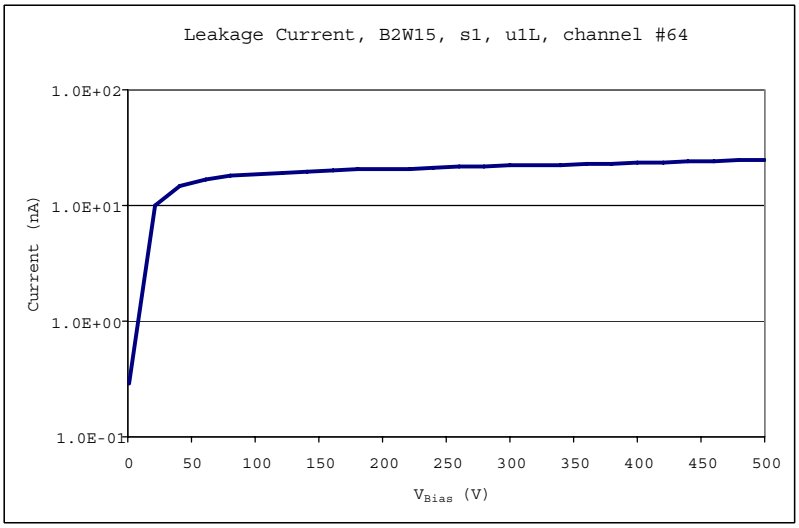

Figure 8: Characteristic plot of leakage current vs bias voltage.

highest possible V_{Bias} being supplied by the power supply was 500V, wheras the voltage is not increased further if the current exceeds a set compliance limit, in this case 2.5 mA (this is the highest possible compliance limit in the 500V range). During the IV measurement on one channel, the other 127 channels are connected to ground.
Doing this for 4 channels per set of pads (48 channels per sensor) gives us the breakdown voltage for all sensors to be

$$V_{Break} > 500V \tag{1}$$

No channels on either sensor were found to have a Breakdown Voltage lower then 500V.

3.3.2 Finding the Depletion Voltage V_{Depl}

To find the bias voltage at which the bulk material is depleted of all free charge carriers, the capacitance is measured as a function of V_{Bias}. A characteristic plot for this is shown in fig.(9). To determine the depletion voltage from this measurement, $1/C^2$ is plotted via V_{Bias} and the Depletion voltage is the voltage

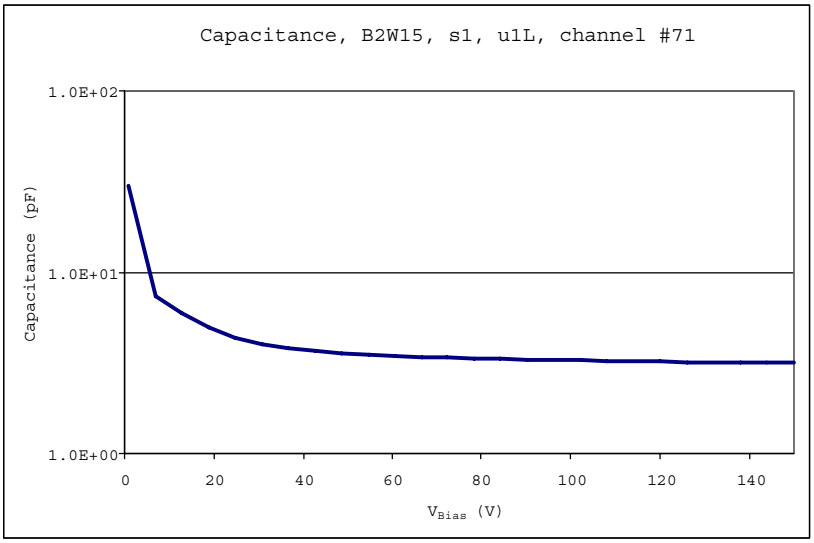

Figure 9: Characteristic plot capacitance vs bias voltage.

at which the curve reaches a constant value. The corresponding plot to fig.(9) is shown in fig.(10). In this case one can see that the depletion Voltage would be

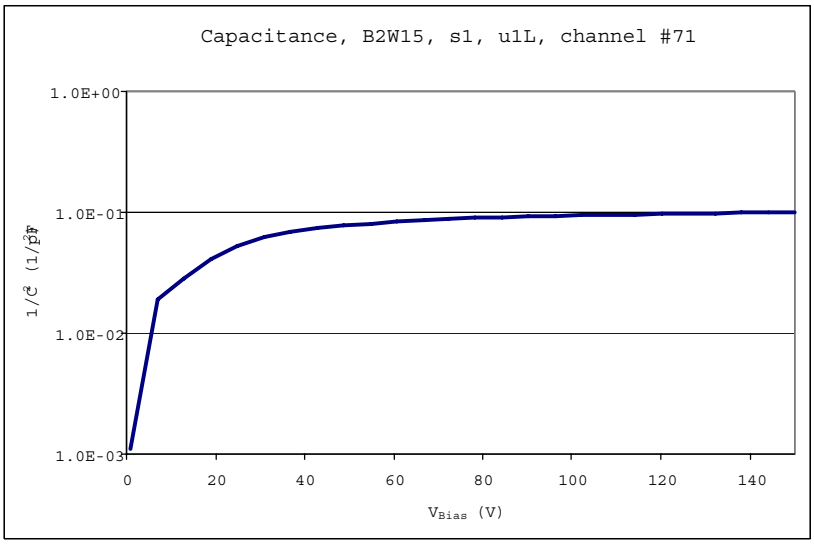

Figure 10: Plot $1/C^2$ vs bias voltage to determine V_{Depl}

$V_{Depl} \simeq 95V$. Nevertheless it should be pointed out that this way of determining the depletion voltage is not defined very well. To find the exact value of the

depletion voltage a different measurement needs to be made in which the sensor is pulsed with a laser. An in depth description of this method is provided in section 4.2.1. Averaging over all V_{Depl}'s for all sensors it is found to be

$$< V_{Depl} >= 95.6V \ , \ \sigma_{Depl} = 30.3V \tag{2}$$

How V_{Depl} scales for the different sensors is summarized in the following table

	$< V_{Depl} >$ (V)	σ_{Depl} (V)
Sensor 1	89.4	14.1
Sensor 2	65.8	8.8
Sensor 3	131.7	21.4

The reason for the big spread of the depletion voltage is that there are no bias resistors in the design of the sensor. Without these bias resistors and no other channels grounded but the ones connected by the probecard, especially channels 1-25 and 103 - 128 have a higher depletion voltage then those in the middle of the set. As two channels were usually closer to the "outside" of the area measured, these would have higher depletion voltages and two closer to the inside would have lower V_{Depl}.
Taking this effect into account, none of the sensors will be measured for leakage current of capacitance below $V_{Depl} + 50V$, to ensure $V_{Bias} > V_{Depl}$ for every channel.

3.3.3 Determining Leakage Current and Capacitance

To determine the leakage current and the capacitance of the sensor under fully depleted conditions, the current and capacitance are measured at an operating voltage of V_{oper} which is chosen as

$$V_{Depl} + 50V < V_{oper} < V_{Break} \tag{3}$$

In the following measurements the operating Voltage was chosen as 200V, putting the sensor well into the fully depleted region of operation but also far away from breakdown conditions. The measurements yielded characteristic plots for the leakage current and capacitance vs channel # as shown in fig.s (11) and (12).
To measure the capacitance of the sensor, two correction measurements needed to be conducted. The first correction was done by the LCR meter (the open correction). This correction measures the extra capacitance due to the attached test fixture. The second correction was obtained by measuring the capacitance of the cables from the LCR meter to the end of the probeneedles. To do this, the probecard was lifted off the sensor and then an AC Scan was run, therefore measuring the correction factor for every channel. This correction was substracted from the measurements later on. The second correction measurement is shown in the following plot, fig.(13): The shape of the correction is due to

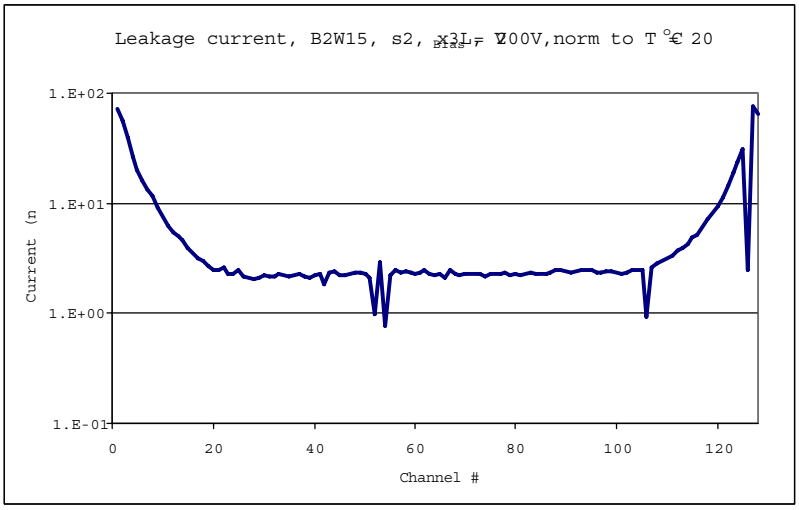

Figure 11: Characteristic leakage current vs channel # plot

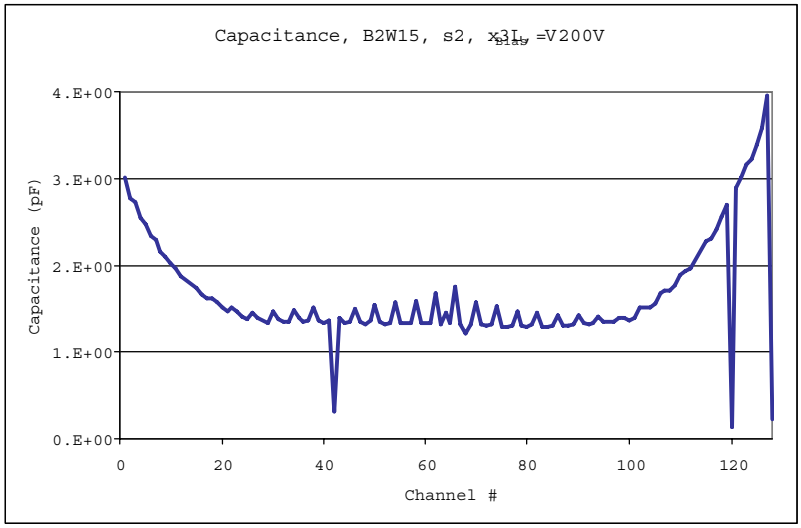

Figure 12: Characteristic capacitance vs channel # plot

the way the connections are made on the probecard. The measurements of the leakage current I_{Leak} and capacitance C are performed on each set of 128 channels, 12 measurements per sensor, on each sensor. All the channels should have approximately the same amount of leakage current and capacitance. This is not the case as can be seen in figures (11) and (12). The first and the last 20 to 30 channels are not on a flat line, but show an increase in leakage current. This is due to these channels bordering the unbiased region of the sensor. This

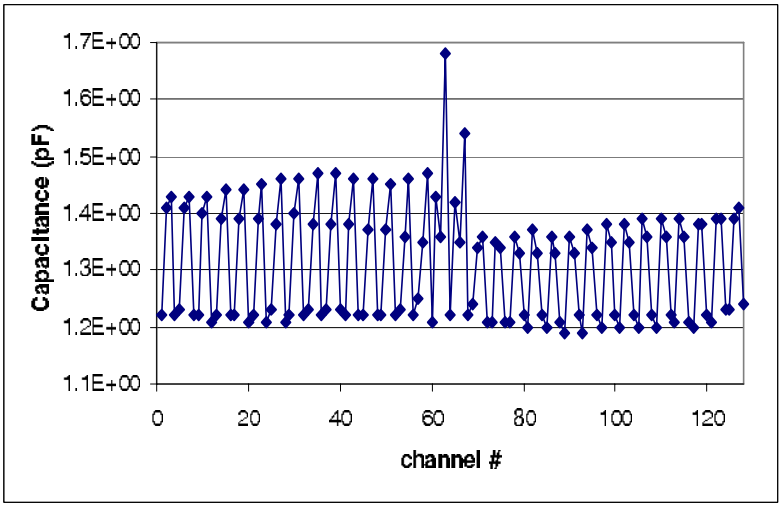

Figure 13: Correction needed to determine the real capacitance of the sensor

means that the parts of the sensor right next to the outside lying channels that are measured, are not depleted of free charge carriers, therefore increasing the leakage current in the channels that are closest to these regions. This situation was resolved as discussed in section 4.1. To get a measure of the leakage current, all the channels that were in the flat part of the curve, between channels 25 and 105 were used to calculate average Leakage current and Capacitance.
Their values were found to be:

$$I_{Leak} = 11.8nA \quad , \quad \sigma_I = 5.5nA \tag{4}$$

$$C = 1.7pF \quad , \quad \sigma_C = 0.3pF \tag{5}$$

The standard deviations are very high, because it was not clear which channels not to use for determining I_{Leak} and C. Again, the individually found leakage currents and capacitances per sensor can be found in the follwing table

	I_{Leak} (nA)	σ_I (nA)	C (pF)	σ_C (pF)
Sensor 1	12.7	11.2	1.8	0.5
Sensor 2	11.2	5.8	1.6	0.2
Sensor 3	11.6	5.5	1.6	0.2

In the following the same measurements were performed with the sensor fully depleted by wirebonding the unmeasured pads to the guardring. This led to major changes in the results.

4 Prototype Characterization Studies

4.1 Electrical Measurements with all sensor channels biased

The left sides of s1 and s2 were grounded by connecting 5 out of the six set of pads to the guardring which is connected to ground through the probecard. To make the wirebonds a wedge type wirebonder was used. The wires have a diameter of $25\mu m$ and are Aluminum 1% Silicon wires. The wedge has dimensions of 64 μm by 102 μm. Due to the size of the wedge, the wirebonds were hard to make precisely, because the size of one pad is only 69 μm by $104\mu m$. A different technique of connecting the pads to the guardring was used. By applying a graphite resistance coating (Aerodag G), a connection between the guardring and the pads was made. The graphite could be easily removed with alcohol after the measurements without damaging the sensor.

4.1.1 Determining V_{Break} and V_{Depl}

The breakdown voltage and the depletion voltage were determined as shown before. The breakdown voltage did not change and the depletion voltage did not change significantly either. To support this, two plots are shown, one for the capacitance and the other for current vs. bias voltage, comparing before and after wirebonding. It can be seen that in fig.(14) the current decreased

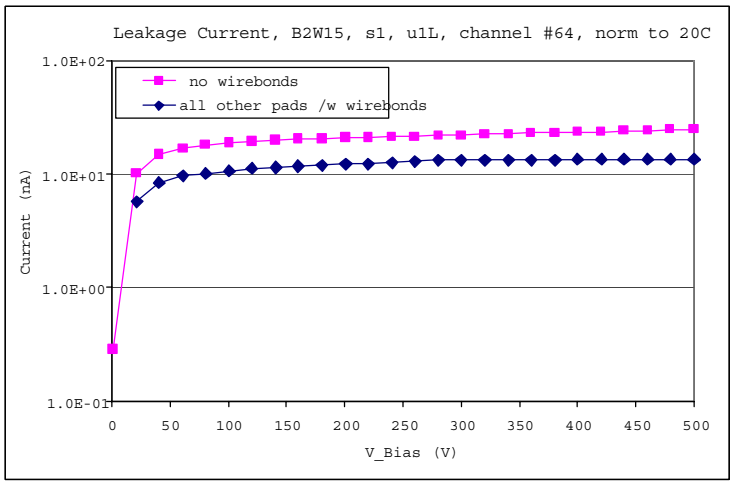

Figure 14: Leakage current vs. V_{Bias} on the fully depleted sensor compared to the results of the sensor without any wirebonds

from the non grounded sensor when wirebonding. But there is no change in the breakdown voltage. In fig.(15) it can be found that the depletion voltage does not change significantly either, but the capacitance decreased when attaching

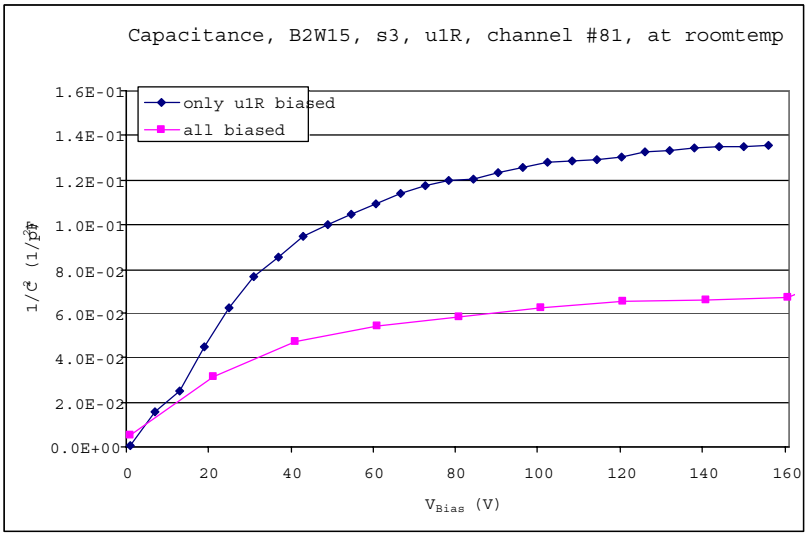

Figure 15: Capacitance vs. V_{Bias} on the fully depleted sensor compared to the results of the sensor without any wirebonds

the wirebonds. Therefore both, V_{Break} and V_{Depl}, were still

$$V_{Break} \geq 500V \tag{6}$$

$$V_{Depl} \simeq 100.2V \ , \ \sigma_C = 26.0V \tag{7}$$

4.1.2 Determining Leakage Current and Capacitance

The leakage current and the capacitance were determined as described before. This time, only two measurements per sensor contributed to the calculation of the average, as the other pads on the sensor were permanently connected to the guardring (not permanently in the case of the graphite, but the connections were not removed either). With these connections in place the typical change of the Leakage Current measurement can be seen in figure (16). This measurement shows the impact of the biasing of the whole sensor on the leakage current. Using all the five measurements taken, one obtains the following value for I_{Leak}:

$$I_{Leak,allbiased} = 3.6nA \ , \ \sigma_I = 3.9nA \tag{8}$$

$$I_{Leak,original} = 11.8nA \ , \ \sigma_I = 5.5nA \tag{9}$$

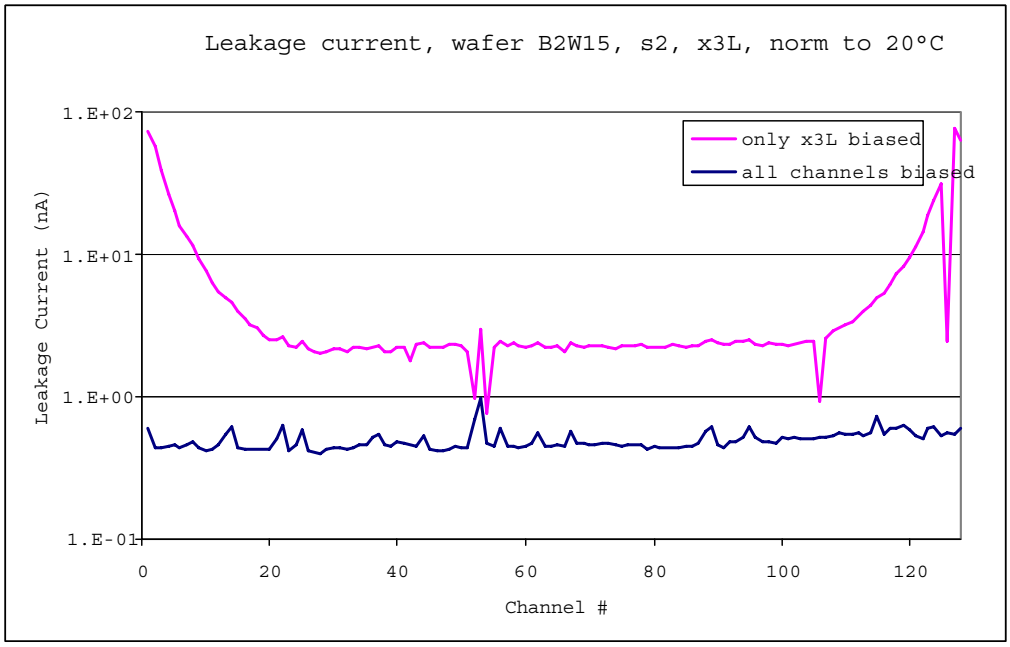

Figure 16: Leakage current vs. channel number on the fully depleted sensor compared to the results of the sensor without any wirebonds

The same is true for the capacitance measurement. Here it is also observed that the complete depletion of the sensor has a significant impact in lowering the value of capacitance. A representative plot is shown in figure (17). With this the average capacitance of the sensor is found to be

$$C_{allbiased} = 1.3pF \quad , \quad \sigma_C = 1.9pF \tag{10}$$

$$C_{original} = 1.7pF \quad , \quad \sigma_C = 0.3pF \tag{11}$$

Both of the values, for the leakage current and the capacitance, are a lot better defined than the previously measured. The leakage current at room temperature is small enough to leave room for irradiation damage (in the case that the detector is kept at 0C.

4.2 Radiation tests

The purpose of the radiation tests was to study the effects of radiation damage on the strip-pixel sensor. In particular on the breakdown voltage, the depletion voltage, the leakage current and the capacitance.

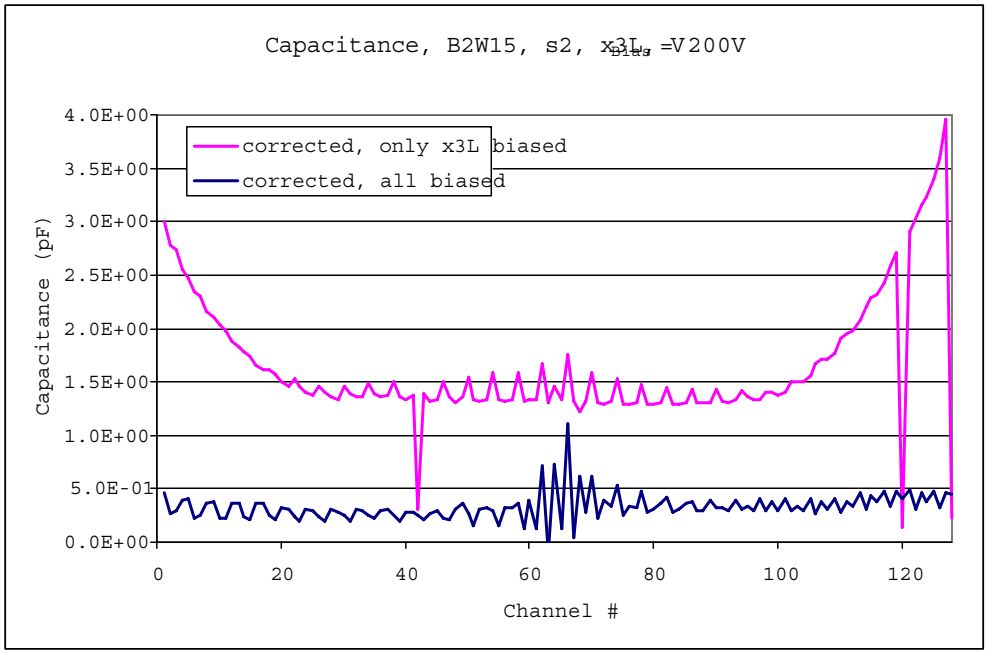

Figure 17: Capacitance vs. channel number on the fully depleted sensor compared to the results of the sensor without any wirebonds

Two of the three available sensors and two of the six testdiodes were irradiated. The sensors/diodes were irradiated at the Indiana University Cyclotron Facility (IUCF) with 200MeV protons. The sensors as well as the diodes were completely emerged in the beam, as the IUCF has the capability to irradiate areas from less than 2cm to 30cm in diameter with a smaller then 30 percent variation of the radiation over the chosen area. The dosimetry at IUCF is routinely better than 10 percent ensuring the accuracy of the chosen doses. Further details of the irradiation are summarized in the following table.

	Irradiation Dose p/cm^2	n-equivalent dose
Sensor 1 / Diode 1U	$5 \cdot 10^{12}$	$4.945 \cdot 10^{12} \pm 4\%$
Sensor 2 / Diode 1D	$5 \cdot 10^{11}$	$4.945 \cdot 10^{11} \pm 4\%$

To calculate the 1MeV neutron equivalent radiation dose, the hardness factor $\kappa_{200MeV,p} = 0.989 \pm 4\%$ for 200MeV protons was used [2].
The specific doses were chosen as they are a good estimate to the expected radiation dose that the detector will experience over the next ten years in RHIC and RHIC II. This was taken from and further measurements of expected radiation doses in the PHENIX IR are currently performed during
RHIC Run 6.
The irradiations were performed at room temperature and no bias was applied

to the sensors and diodes during irradiation. After the irradiation, the sensors/diodes were kept in a $-17°$ freezer, shipped to UNM in dry ice and again kept in a $-20°$ freezer until measured. During the measurements a thermal chuck was used, keeping the sensors/diodes at about $-1°$C. The setup for the measurements was the same, but the cold chuck was added between the sensor and the bottom chuck (see fig(13)).

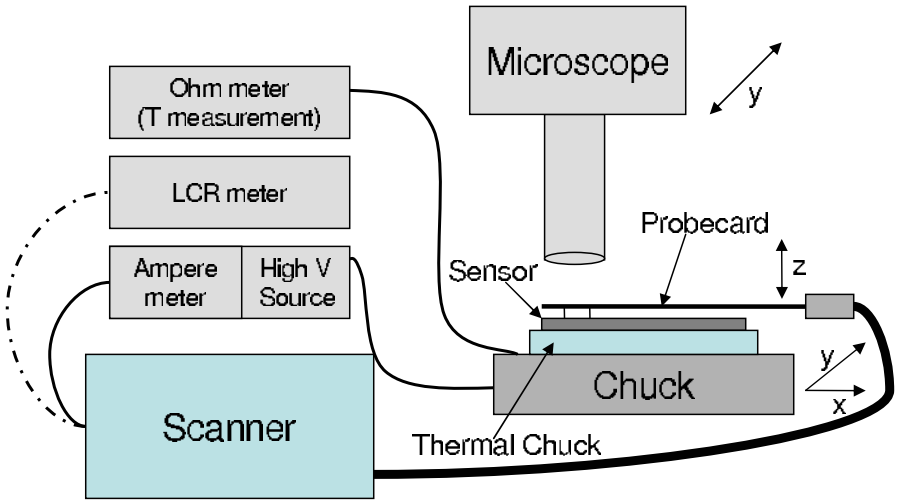

Figure 18: Setup of the Probestation with thermal chuck

The diodes were measured first. The purpose of measuring the diodes was to use them as a control to find the actual fluence levels obtained during irradiation. IV measurements were made at $-1°C$ and the results were normalized to $20°C$ according to the equation $I(T) \propto T^2 \cdot e^{-\frac{E}{2kT}}$. E is the effective energy gap, T is the measured temperature and k is Boltzmann's constant.

4.2.1 Irradiated Diodes

To measure the diodes the probecard was replaced with a single probe (the scanner was not used) and IV and CV curves were measured. As before, V_{Break} was determined from IV and the CV measurements were used to find V_{Depl}. After the initial measurements the diodes were annealed at $60°C$ for 80min and the measurements were repeated. The results from the annealed diodes are presented first, because they are used to identify the real equivalent flux from the results of the non annealed diodes.
The results from the CV measurements were inconclusive for the annealed and pre-annealed diodes, because of the missing guard ring on the diodes. The results of the CV measurements are shown in fig.(19) and it is seen that they keep rising with increasing V_{Bias} due to the lateral depletion that exists because of the non-contained electric field.
A different technique to determine the depletion voltage for the diodes was used.

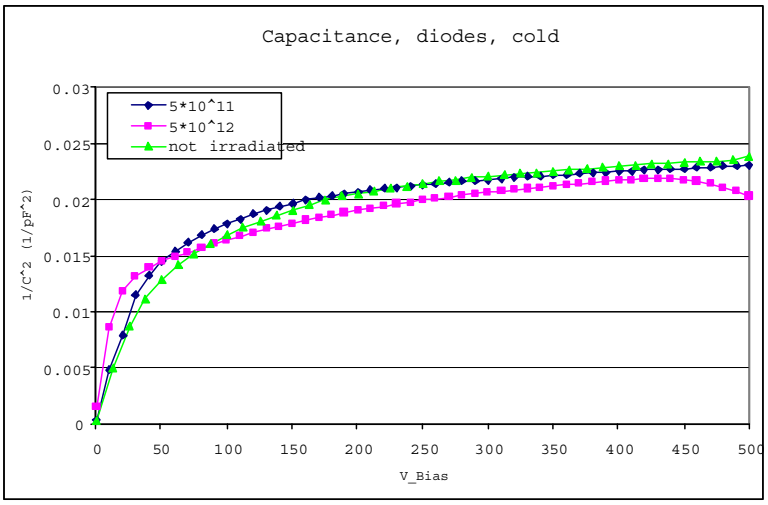

Figure 19: Capacitance of the diodes, measured at $0°C$

The setup for this measurement is shown in fig.(20). For this measurement a

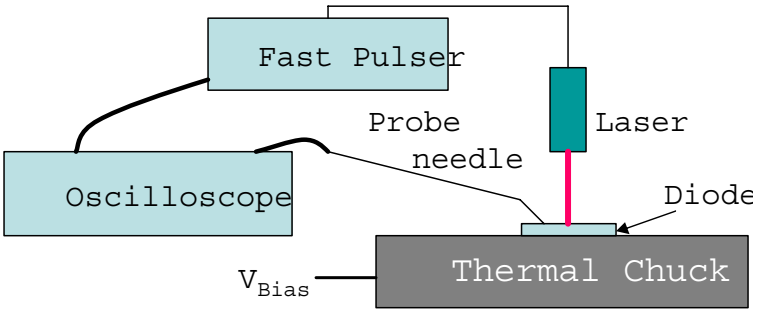

Figure 20: Setup for measuring the Depletion voltage of the Diodes

1064nm wavelength laser beam with a spot diameter of about 1mm is was shone onto the middle of the diode. The signal was then readout with a probeneedle connected to an oscilloscope. The output of the fast pulser was also read out to the oscilloscope to show the trigger signal. Then the pulseheight was measured on the oscilloscope while the bias voltage V_{Bias} was increased. The depletion voltage is defined here as the value of V_{Bias} when the pulse height stops increasing.

The results from this measurement are shown in fig.(21) and it is clear that the depletion voltage result is much more clear. It is about the same for all the three diodes independent of their received radiation dose, namely

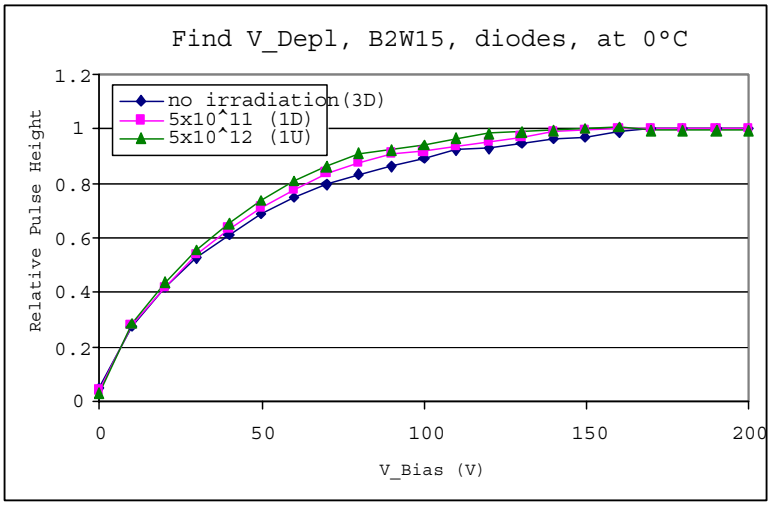

Figure 21: Measuring the pulseheight of the signal from the diode being pulsed by a laser

$$V_{Depl,Diodes} \simeq 120V \tag{12}$$

Next the leakage current on the annealed diodes was measured and the results are presented in fig.(20).
The damage parameter α after annealing at $60°C$ for 80min is constant [3] at

$$\alpha_{80/60} = 4.0 \cdot 10^{-17} A/cm \pm 4\%. \tag{13}$$

Using the leakage currents at $V_{Bias} = 200\text{V}$ ($> V_{Depl}$), the constant α and the Volume of the diodes (Vol $= 4mm \cdot 4mm \cdot 0.5mm \pm 10\%$), the equivalent fluences can be calculated using

$$\alpha = \frac{\Delta I}{Vol \cdot \Phi_{equ}} \tag{14}$$

This gives the following values for the equivalent fluences

$$\Phi_{equ,1} = (4.251 \pm 0.458) \cdot 10^{11} cm^{-2} \tag{15}$$

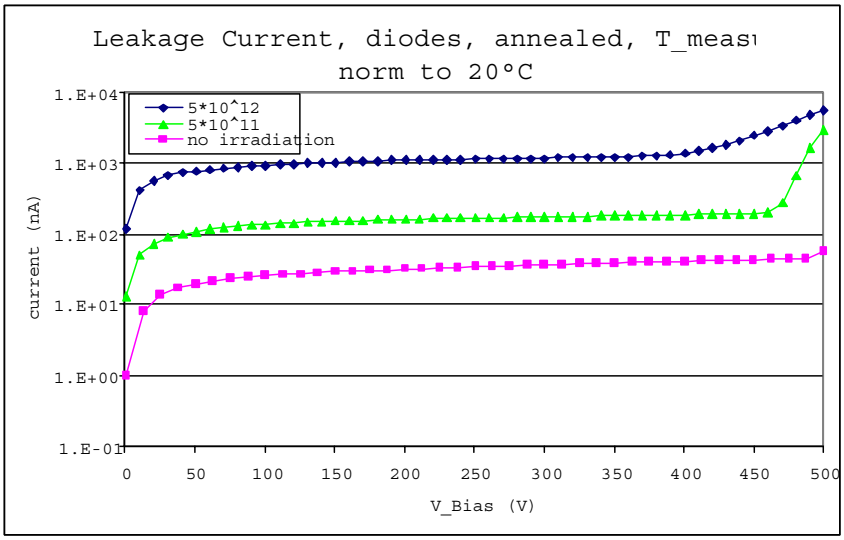

Figure 22: Measuring the leakage current of the annealed diodes

$$\Phi_{equ,2} = (3.472 \pm 0.374) \cdot 10^{12} cm^{-2} \tag{16}$$

Φ_{proton} is then calculated via $\Phi_{proton} \cdot \kappa_{200MeV,p} = \Phi_{equ}$ and all the different fluences compare as follows

	Measured (cm^{-2})	Target (cm^{-2})	Irrad. Lab Dosimetry (cm^{-2})
$\Phi_{proton,1}$	$(4.298 \pm 0.494) \cdot 10^{11}$	$5.0 \cdot 10^{11}$	$5.004 \cdot 10^{11} \pm 10\%$
$\Phi_{proton,2}$	$(3.511 \pm 0.403) \cdot 10^{12}$	$5.0 \cdot 10^{12}$	$5.001 \cdot 10^{12} \pm 10\%$

Now it is known how the fluences really scaled and these numbers will be used instead of the ones that were given by the irradiation Lab.
The IV curve for the pre-annealed diodes was also measured and is shown in fig.(21). From this, the damage parameter α was also calculated (using the currents at $V_{Bias} = 200$V). This α is found to be

$$\alpha_{0/60} = (4.589 \pm 0.254) \cdot 10^{-17} V/cm \tag{17}$$

As expected, the $\alpha_{0/60}$ is larger than the post-annealing $\alpha_{80/60}$.

4.2.2 Irradiated Sensors

The measurements performed on the sensor are going to reveal the effects of the irradiation on breakdown and depletion voltage as well as leakage current and

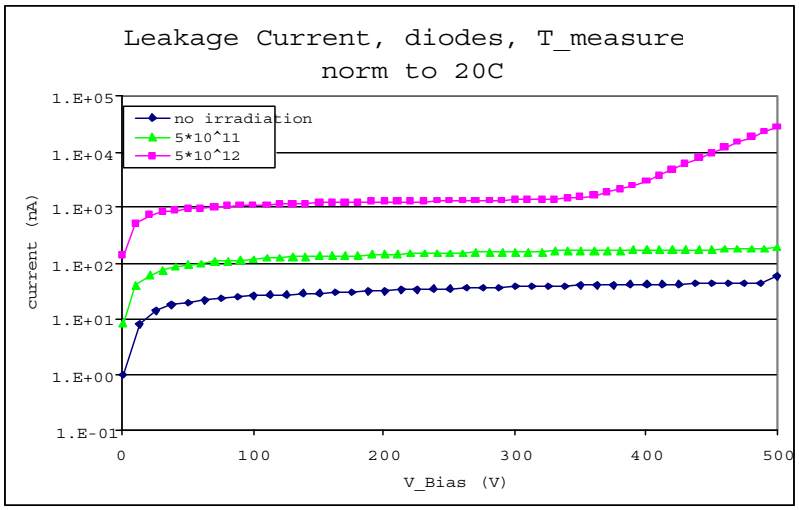

Figure 23: Measuring the leakage current of the irradiated diodes pre-annealing

capacitance. One would expect to see similar results to the ones obtained on the diodes. Similiar to the diodes, the sensors were annealed for 80min at $60°C$ and measurements were taken before and after annealing. This time, sensor 1, which was irradiated to $5 \cdot 10^{12} cm^{-2}$, was not measured pre-annealing because the currents were too high and the thermal chuck used could only cool the sensor to $-1°C$. Therefore, only the measurements post annealing are discussed.
To measure the sensors, all the readout pads were again biased. Measurements without grounding the other areas of the sensors were not taken as the leakage current was too high in this case.
The measurements performed were the same as on the non-irradiated sensors, an IV-scan to find V_{Break}, a CV-scan to find V_{Depl} and a complete current and capacitance scan at fixed V_{Bias}. The results are presented and discussed in the following. All the measurements were taken at $0°C$ for the $5 \cdot 10^{11} cm^{-2}$ sensor and at $-10°C$ for the $5 \cdot 10^{12} cm^{-2}$ sensor, the IV results normalized to $+20°C$ as discussed in section 3.5.

Breakdown Voltage The IV-measurements to find the breakdown voltage were performed on individual strips. All the other sensor channels were biased (with wirebonds or graphite). The IV-curves for all three sensors are plotted below in fig.(24). It is already known that the breakdown voltage for the non irradiated sensor is $> 500V$. From the IV measurements it can be seen that the breakdown voltage for s2 ($5 \cdot 10^{11}$) is at $\boxed{V_{Break} \simeq 280V}$. The measurement for s2 stops at 280V, because the whole sensor breaks down at this voltage and exceeds the highest possible compliance limit on the ammeter. The same happens for s1 ($5 \cdot 10^{12}$) at $\sim 250V$. The difference for s1 is, that no rise in the IV curve is seen at 250V, so the breakdown voltage stays unknown for this sensor.

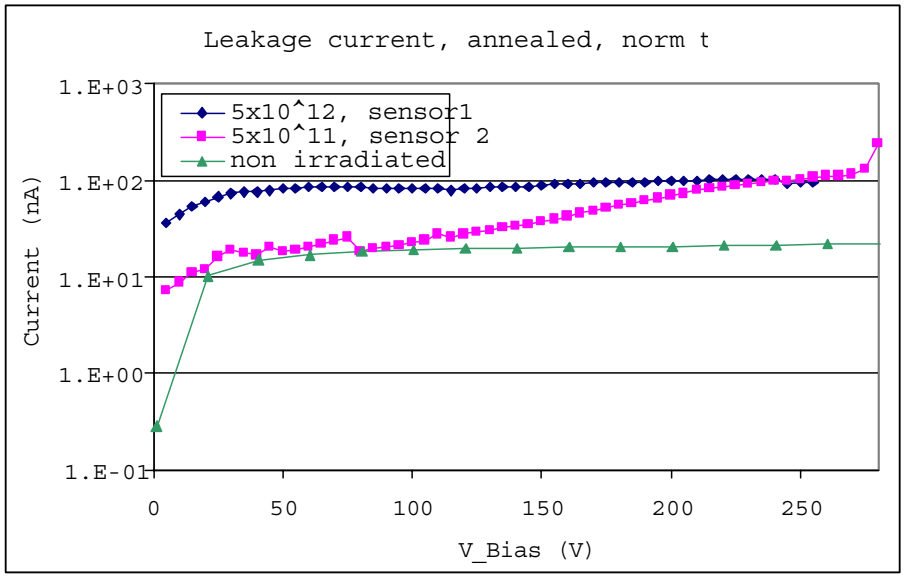

Figure 24: Measuring the leakage current of the irradiated sensors post-annealing

The IV curve for the entire sensor can be plotted as well, showing the breakdown at 250V (see fig.(25)): The "bump" in the data between 50 and 120V is due to noise induced by the thermal chuck. Any measurement performed showed some effect of the noise on the measurements, so no results without the disturbances are presented. It should be noted here, that the currents drawn by the entire sensors are particularly high. Even at very low bias voltages, the current already exceeds 1mA.

Depletion Voltage The Depletion Voltage is measured using the two methods discussed earlier: By measuring the CV curve with an LCR meter and by measuring the signal pulse height on the oscilloscope while laser pulsing the sensor. Again, the measurements are performed on a single strip with all the other sensor channels biased. The results for the CV measurements are shown in fig.(26). From this, the depletion voltage for s2 is $\boxed{V_{Depl} \simeq 100V}$ and for the non-irradiated sensor $\boxed{V_{Depl} \simeq 120V}$. The depletion voltage for the highly irradiated sensor can not be determined using this method, due to the same reasons that the IV measurement had to be stopped early.
Using the laser setup with the unfocused beam of about 1mm diameter and the oscilloscope to read out the pulse height, the measurements shown in fig.(27) were taken: It can be seen that the depletion voltage can be easily found using this method: s2 has depletion Voltage of $V_{Depl} \simeq 95V$, s1 has $V_{Depl} \simeq 160V$ and the non irradiated sensor has $V_{Depl} \simeq 110V$.

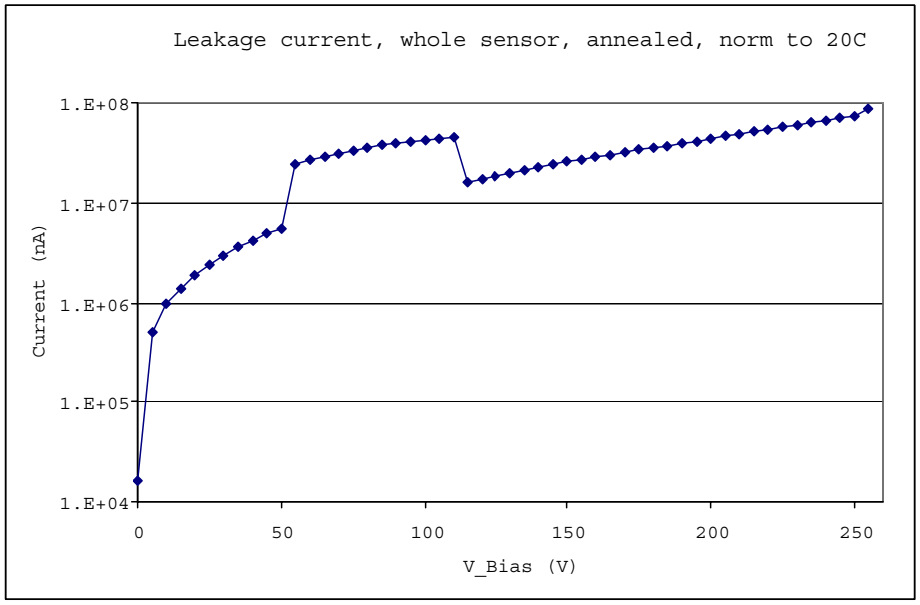

Figure 25: Measuring the leakage current of entire sensor 1 post-annealing

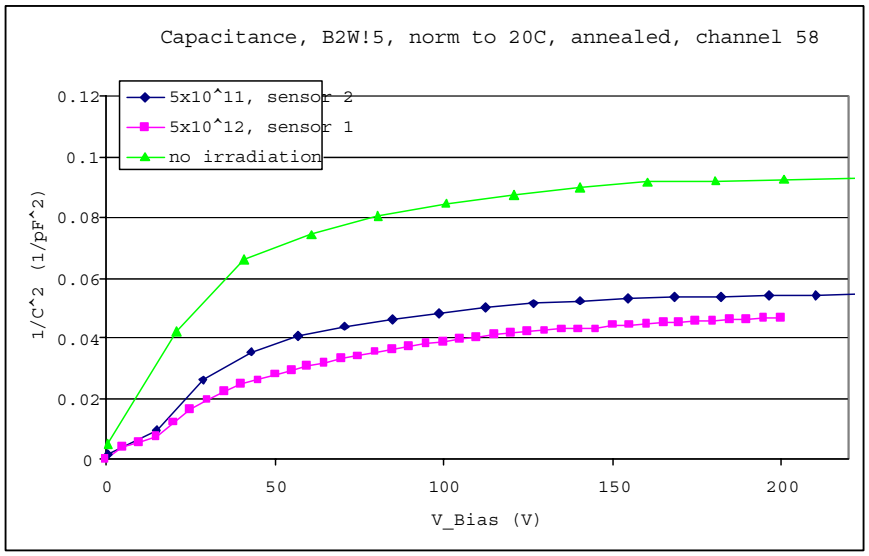

Figure 26: Measuring the capacitance of the irradiated sensors post-annealing

Summarizing the results from IV and CV/laser measurements:

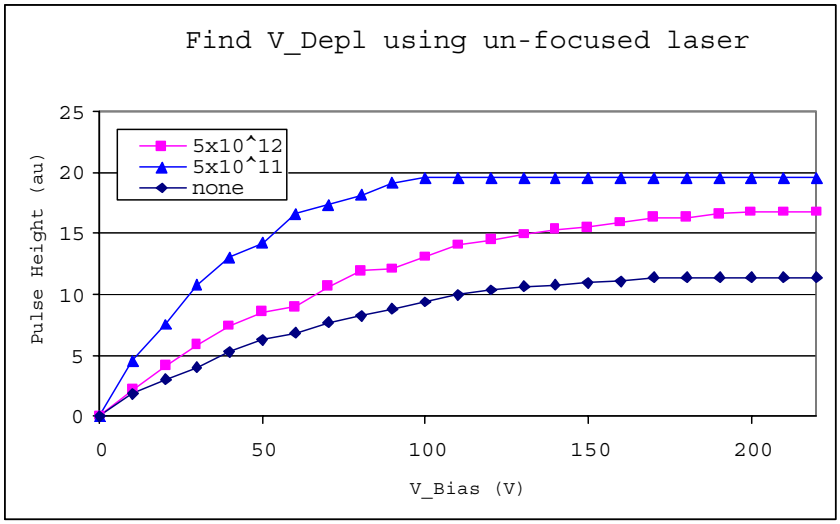

Figure 27: Finding V_{Depl} using the readout pulseheight of an IR laser

Radiation Dose	V_{Break}	V_{Depl} (CV Scan)	V_{Depl} (Laser Probing)
s3, non irradiated	$\geq$ 500V	120V	110V
s2, $4.298 \cdot 10^{11} cm^{-2}$	$\simeq$ 250 V	100V	95V
s1, $3.511 \cdot 10^{12} cm^{-2}$	no measurement	no measurement	160V

The obtained values for the depletion Voltage can also be plotted versus the radiation fluence which is shown in fig.(28). This result implies that the highly irradiated sensor went through type inversion, increasing the depletion voltage from the non irradiated sensor. The sensor that was irradiated with the lower dose is still on the beneficial side of the annealing [3].

Leakage Current The Leakage current scan was performed on a different cold chuck than the single channel measurements, so that the measurement temperature is $0°C$. One whole set of 128 channels is measured and all other sensor channels are again biased. The results of these measurements are plotted in fig.(29). Only the channels from 40 to 100 are considered for determining the leakage current I_{Leak}, because the other channels are too noisy or showing abnormal features. With this the $20°C$ normalized leakage currents are found to be:

Radiation Dose	I_{Leak} (nA)
non irradiated	$\simeq$ 1.5
$4.298 \cdot 10^{11} cm^{-2}$	$\simeq$ 4.3
$3.511 \cdot 10^{12} cm^{-2}$	$\simeq$ 60.8

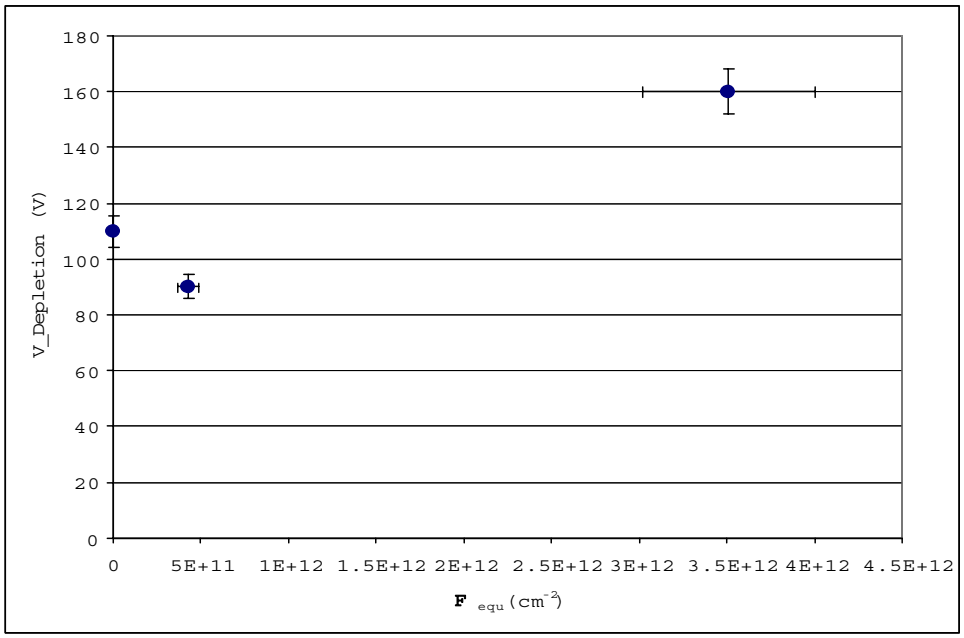

Figure 28: Plotting V_{Depl} vs the radiation fluence

When plotting I_{Leak} vs the radiation fluence, the slope of the line should be equal the damage parameter α divided by the volume under one strip Vol_{Strip}. This volume can be estimated and also found from the plot of Φ_{equ} vs $\Delta I/Vol$, because as the measurements were performed after annealing the sensors, α again has to be $4 \cdot 10^{-17} A/cm$.
The volume under one strip can be estimated as follows. One pixel has two spirals of p+ implant interleaving. They are identical to each other, but one is rotated by 180° with respect to the other. So half of the volume of one pixel should correspond to the volume of one pixel for one strip. The volume of one pixel is calculated from its width $w = 0.08mm$, its length $l = 1mm$ and its thickness of $d = 0.5mm$. It also has to be considered that 30 pixels are connected together to give one strip-pixel, so the volume can be estimated as:

$$Vol_{strip,est} = \frac{1}{2} \cdot 0.08mm \cdot 1mm \cdot 0.5mm \cdot 30 = 0.6 \cdot 10^{-4} cm^3 \qquad (18)$$

Accounting for the gaps between the p+ implants, this value for the volume should approximately be devided by a factor of 2. Then the estimated volume will be

$$Vol_{strip,est} \simeq 0.3 \cdot 10^{-4} cm^3 \qquad (19)$$

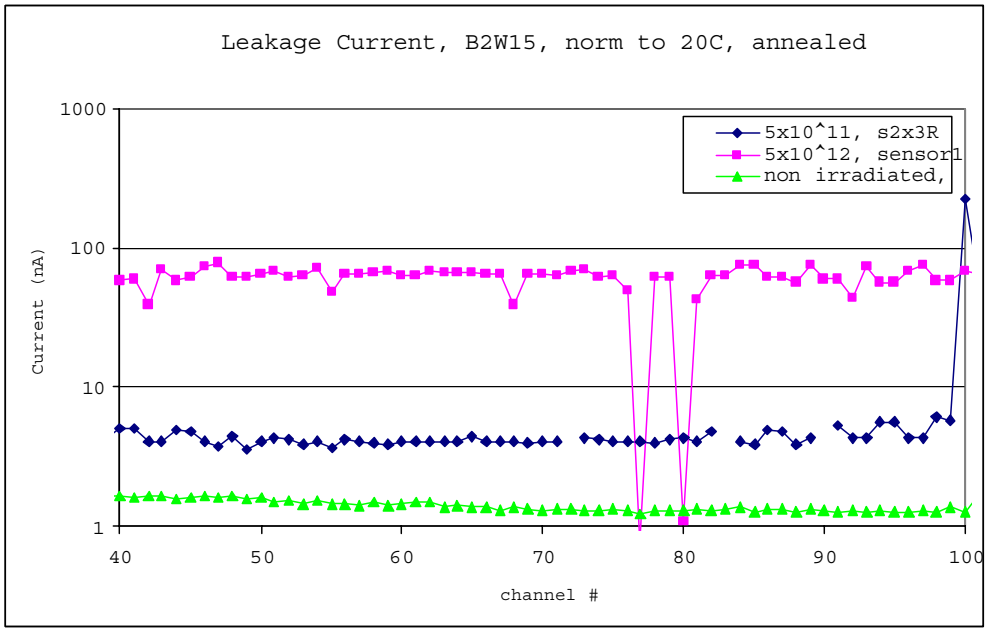

Figure 29: Leakage current vs channel number at $V_Bias = 200V$

Using the calculated volume $Vol_{strip,calc}$, $\Delta I/Vol_{Strip,calc}$ vs Φ_{equ} can be plotted to see if it corresponds to the universally found plot [3]. This is shown in fig.(30).
To a good approximation, the data points lie on the universal line, therefore confirming that the measurements agree with the universal idea.

Capacitance As already done in the Leakage Current section, the capacitances before and after irradiation will be compared. Again, one set of pads was measured on the thermal chuck at $0°C$. For the same reasons as discussed before, only channels 40-100 are considered in finding the average capacitance. The measurement results are shown in fig.(31).

Using these results, the capacitances pre- and post-irradiation are found as:

radiation dose	Capacitance (pF)	σ_C (pF)
no irradiation	0.4	
$5 \cdot 10^{11} cm^{-2}$	1.2	
$5 \cdot 10^{12} cm^{-2}$	1.3	

The Capacitance seems to increase when the sensors are irradiated. This is important to remember when considering the readout electronics, to make sure they can handle the capacitance increase.

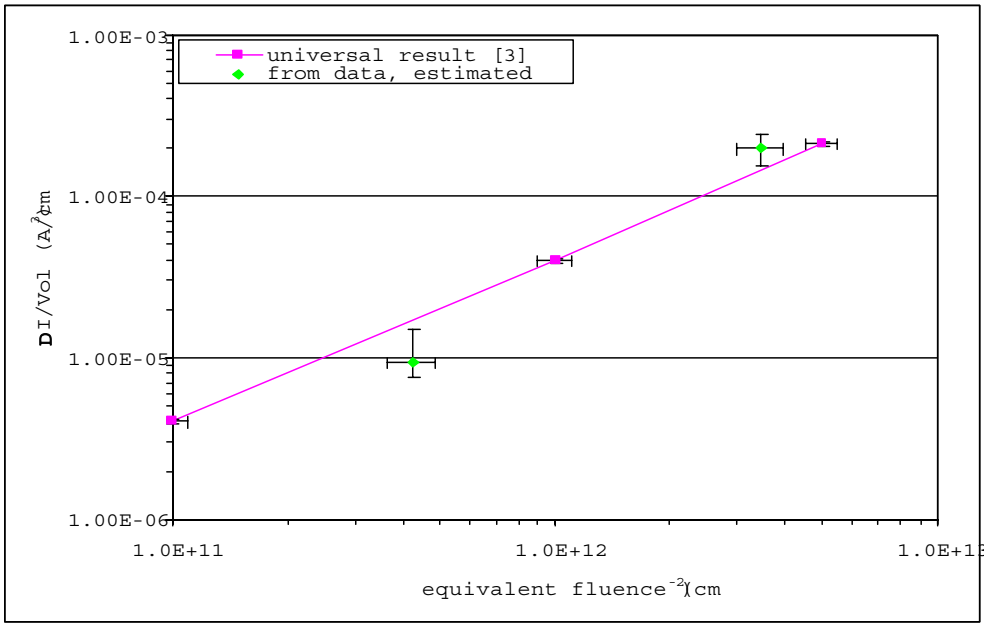

Figure 30: Comparing the results of the universal line for leakage current per volume vs. fluence

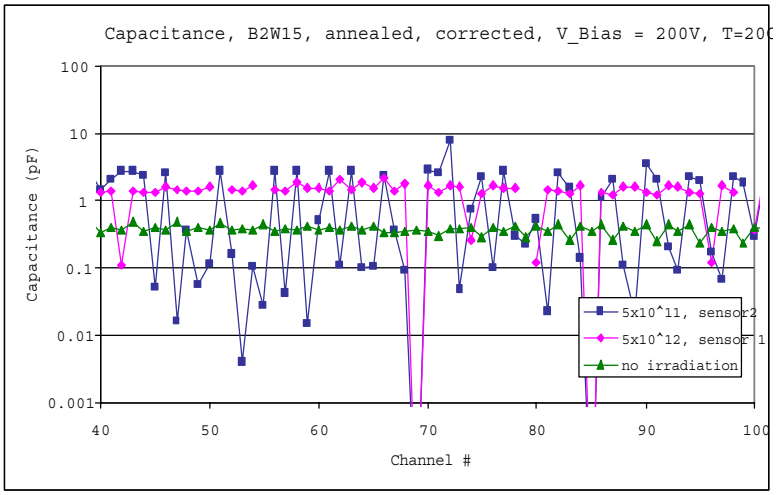

Figure 31: Capacitance measurements on the non irradiated and the irradiated sensors compared

4.3 Laser Tests

The laser pulse studies were performed on the sensors pre and post irradiation. The setup for the study is shown in fig.(32) The sensors are placed on a ther-

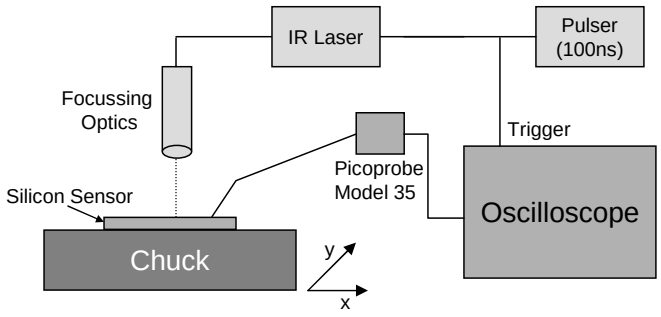

Figure 32: Setup of the laser test station

mal chuck and a collimated laser beam with a spotsize of about 5 - 10 microns FWHM is focused on the sensor. The laser spot is focused using the microscope, making it possible to exactly position the spot on the sensor. The probeneedles used to read out the sensor both have preamplifiers attached to make the readout of a signal possible (the spot size is too small to create a signal that can be read out without the amplifiers).
Two sensor channels are chosen to be read out and all the other channels are biased during the measurement. The two channels are chosen so that they have one pixel in common. This means that they have to have one pixel where the first readout channel corresponds to the u strip and the second to the x strip. This is also described in fig.(33), where a laser spot is shown as well.

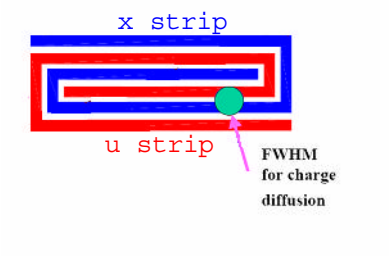

Figure 33: Interleaving Pixel and Laser Spot

The laser spot is always positioned in the gap between the first pixel and the guardring and then scanned in x direction over the first pixel (x being the direction of the smaller width of the pixel). The Bias Voltage is set to 200V in all the three different cases. The results for the non irradiated sensor and the two irradiated sensors are shown in fig.s (34)-(36).
In fig.(35) it needs to be explained what bigger spot size means. As mentioned

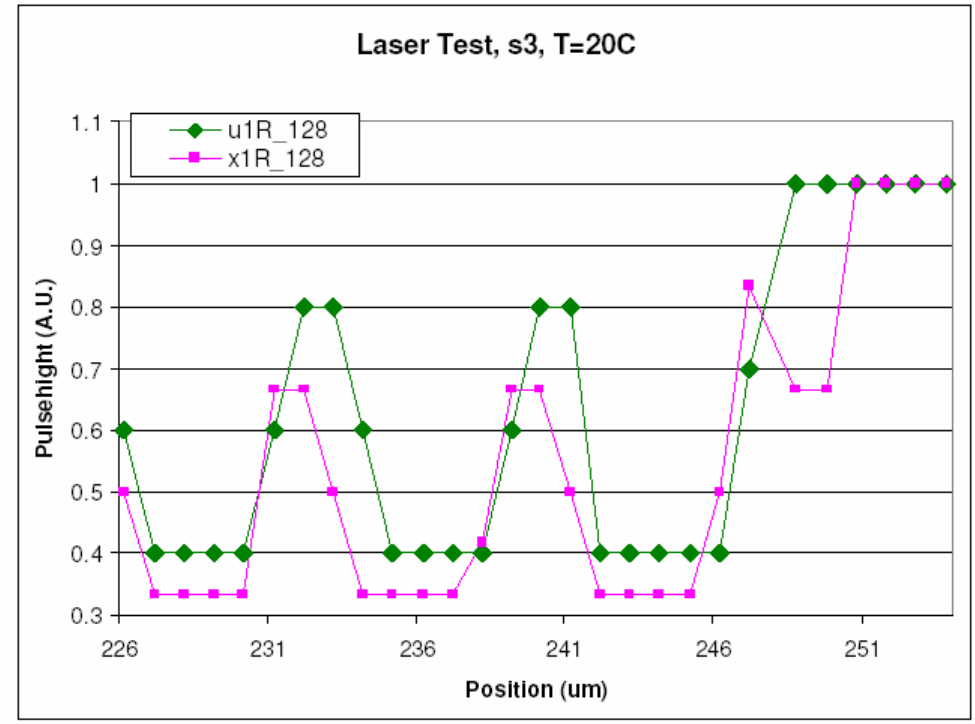

Figure 34: Laser pulse study, non irradiated sensor

before, s2 suffered some damage inflicted on the sensor after irradiation due to problems with the probestation. It was necessary to increase the laser spot in order to increase the signal on the readout strips. It should also be noted that the sensor performs well after irradiation. A strong signal on both the x- and u-strips is observed.
The position of the Aluminum strips can also be easily identified. Due to its wavelength the laser is not able to penetrate the Al strips and a signal is only observed when the laser is positioned in between the aluminum. It should be noted here that these studies do not determine charge dispersion in the silicon since other effects such as reflection of the laser light from the back side metalization cannot be easily determined. Precise charge sharing studies are normally done in beam with precise tracking.

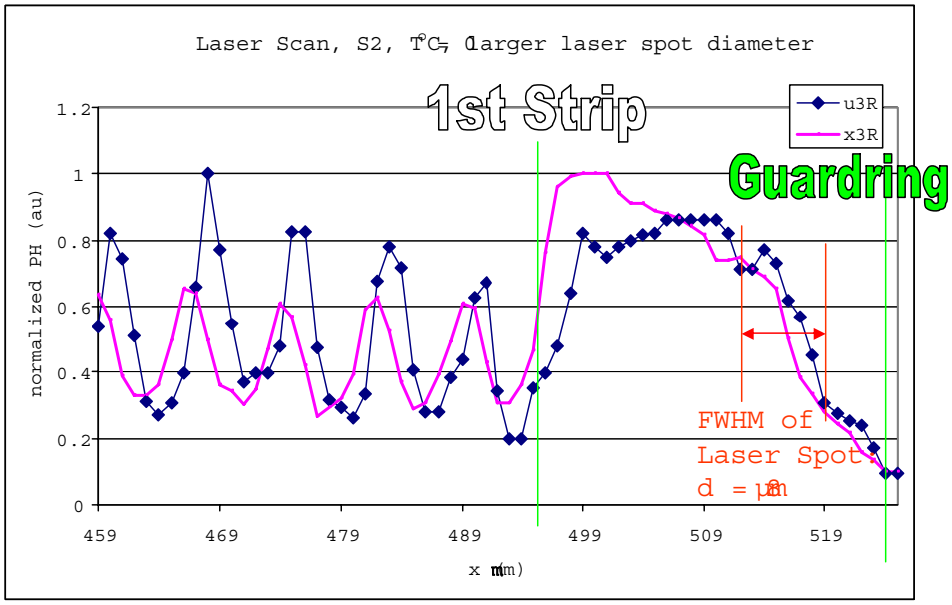

Figure 35: Laser pulse study, $\Phi_{200MeV,p} = 4.251 \cdot 10^{11}$

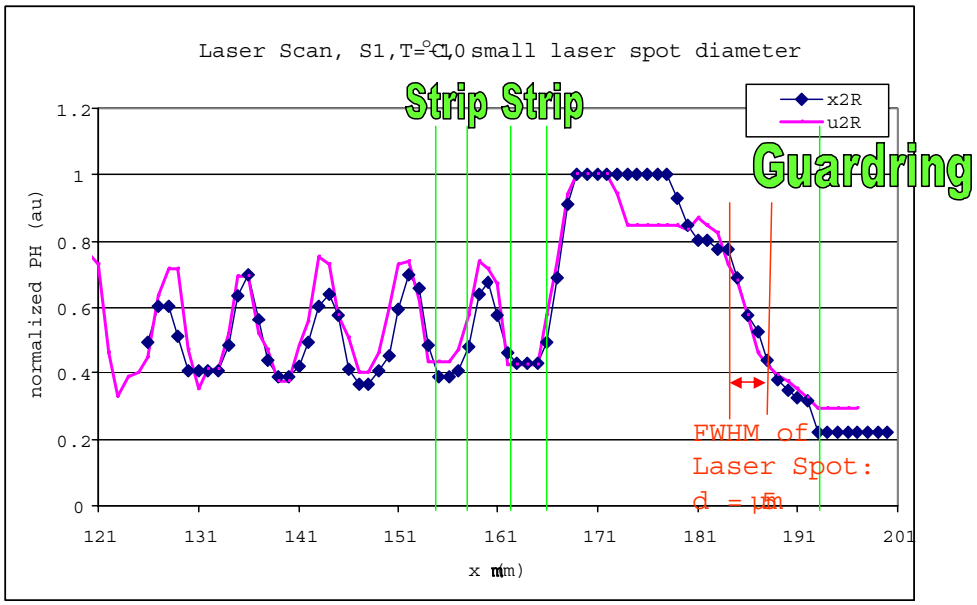

Figure 36: Laser pulse study, $\Phi_{200MeV,p} = 3.472 \cdot 10^{12}$

5 Conclusions

The irradiation studies at UNM have showed that the preproduction strip-pixel sensors show an increase in leakage current as a functio of the radiation damage which is consistent with expectations. These levels of increase in leakage current may be a problem for the electronics if the detector is not cooled during operation. The lack of bias resistors on the sensors makes meaningful testing problematic and should be considered for the final design.

6 Recommendations

There are a couple of minor improvements that need to be made on the sensors to enhance their usability. There needs to be a guardring added to the diodes on the wafers and a second scratch pattern for sensor identification needs to be added to the design of the sensor to ensure foolproof identification of each sensor. There is also a need to include bias resistors on the sensor design. If this is not possible, the information from strip-by-strip QA testing has limited usefullness before bonding to the electronics. We recommend that Hamamatsu perform the tests with the 128 needle probe card, and then, based upon the pass rate determined from statistical sampling, a certain percentage of strips should be re-tested. To determine the pass rate, more statistics are needed on fully biased sensors.
In general, more tests need to be performed on the sensors available to confirm testing programs and to give a better statistics on bad channels/ bad sensors before the production sensors are tested.

References

[1] Z.Li, et.al., "Novel silicon stripixel detector for PHENIX Upgrade", NIMA 518 (2004) 300-304

[2] http://sesam.desy.de/members/gunnar/Si-dfuncs.html

[3] G. Lindström, M. Moll, E. Fretwurst, "Radiation hardness of silicon detectors - a challenge from high-energy physics", NIM A 426 (1999) 1-15